Supporting Information

Controlled ROS generation in pyridinium-functionalized nanocatalysts for selective photooxidation

Jing-Wang Cui,[a,b] Shuai Ma,[a] Yun-Rui Chen,[a] Jia-Qi Pan,[a] Bin Tan[a] and Jie Zhang*[a]

[a] *MOE Key Laboratory of Cluster Science, School of Chemistry and Chemical Engineering, Beijing Institute of Technology, Beijing 102488, P. R. China.*

[b] *Beijing Key Laboratory of Solid State Battery and Energy Storage Process, State Key Laboratory of Mesoscience and Engineering, CAS Key Laboratory of Green Process and Engineering, Institute of Process Engineering, Chinese Academy of Sciences, Beijing 100190, P. R. China.*

**Corresponding author: Jie Zhang*

E-mail: zhangjie68@bit.edu.cn

Table of contents

Section 1. Experimental procedure

1.1 Materials and instructions

All chemicals and reagents were purchased from commercial sources and were of GR/AR grade unless otherwise noted. The solvent used in photocatalytic experiments was chromatographically acetonitrile. The ultrasonic treatment was performed in a KQ2200B ultrasonic bath (100 W, 40 kHz). The multichannel photochemical reaction systems (PerfectLight PCX50C for 365 nm light, SSSTECH-LAL1CV1.0 for 395 nm and white light) were used for photocatalytic reactions. Infrared (IR) spectra were measured in the range of 4000-400 cm^{-1} on a Nicolet iS10 FT-IR spectrometer with samples prepared as KBr pellets. Elemental analysis (EA) of C, H, and N was investigated on a Vario EL III CHNOS elemental analyzer. The scanning electron microscopy (SEM) image and energy-dispersive X-ray spectroscopy (EDS) mapping were studied on a JSM-6700F scanning electron microscope. The atomic force microscopy (AFM) image was measured by a JSM-6700F scanning electron microscope. Powder X-ray diffraction (PXRD) patterns were recorded on a Bruker D8 Advance X-ray diffractometer with Cu Kα radiation (λ = 1.5406 Å). The UV-Vis absorption properties were monitored by a PE Lambda 900 spectrometer. Thermogravimetric analysis (TGA) was researched on a Mettler Toledo TGA/DSC 1/1100 analyzer under air an atmosphere with a heating rate of 20 °C min^{-1} from 30 to 1000 °C. ^{1}H NMR spectra were characterized on a Bruker AV-400 NMR spectrometer by dissolving samples in deuterated reagent (DMSO-d_6). X-ray photoelectron spectroscopy (XPS) studies were conducted with a PHI 5000 Versaprobe III X-ray photoelectron spectrometer using Al Kα radiation (X-ray beam spot 200 μm). The XPS fitting was calculated by MultiPak-9.8 software. Electron spin resonance (ESR) measurements were carried out using a JES-FA200 ESR spectrometer. Dynamic laser scattering (DLS) was analysed by Malvern Zetasizer Nano ZS. Gas chromatography (GC) analysis was operated on Shimadzu GC-2014C with a FID detector equipped with an Rtx-5 capillary column.

1.2 Synthetic procedures

1.2.1 Synthesis of L-COOH·Cl

4'-(4-pyridyl)-2,2':6',2''-terpyridine (**PTP**) (3.10 g, 0.01 mol) and 4-(chloromethyl)-benzoic acid (3.42 g, 0.02 mol) were mixed in 40 mL of *N*,*N*-dimethylformamide. The mixture was heated under 110 °C for 8 h, and then filtered while still hot. The white powder was obtained in 65% yield. ^{1}H NMR (400 MHz, DMSO-d_6) (Figure S1): δ 13.17 (1H, s), 9.40 (2H, d, J = 8.0 Hz), 8.92 (2H, s), 8.84 (2H, d, J = 8.0 Hz), 8.81 (2H, d, J = 4.0 Hz), 8.72 (2H, d, J = 8.0 Hz), 8.10 (2H, m), 8.03 (2H, d, J = 12.0 Hz), 7.68 (2H, d, J = 8.0 Hz), 7.60 (2H, m), 6.06 (1H, s).

1.2.2 Synthesis of Cd-L-COO ($[Cd(L\text{-}COO)Cl_{0.644}(NO_3)_{0.356}]\cdot OH\cdot 4H_2O$)

L-COOH·Cl (19.96 mg, 0.04 mmol) that the pH value has been adjusted to 7.0 by using 0.1 M NaOH aqueous solution in 2.5 mL of water was added into a 25 mL glass bottle containing 2.5 mL of aqueous solution of $Cd(NO_3)_2\cdot 4H_2O$ (24.64 mg, 0.08 mmol). After stirring for 30 min at room temperature, the mixture was sealed, heated under 110 °C

for 3 days, and then cooled down to room temperature. The pink bulk crystals were generated in 68% yield.

1.2.3 Synthesis of Cd-L-COO-NP through the ultrasonication

The resulting nanoparticles were got by the ultrasonication of a 25 mL glass bottle containing **Cd-L-COO** (4.00 mg) and acetonitrile (5 mL) at room temperature for various times (15 min, 30 min, and 45 min) in the ultrasonic bath (100 W, 40 kHz).

1.2.4 Synthesis of L-COO

L-COOH·Cl (19.96 mg, 0.04 mmol) was added into a 25 mL glass bottle containing 5 mL of H_2O/DMF solution (3:2, v/v). The mixture was sealed, heated under 95 °C for 1 day, and then cooled down to room temperature. Next the mixture was transferred to an oven at 32.5 °C and volatilized until colorless rod-like crystals appeared. The yield of **L-COO** is calculated as 73%. ^{1}H NMR (400 MHz, DMSO-d_6) (Figure S1): δ 9.37 (2H, d, J = 8.0 Hz), 8.92 (2H, s), 8.82 (2H, d, J = 8.0 Hz), 8.80 (2H, d, J = 4.0 Hz), 8.72 (2H, d, J = 8.0 Hz), 8.09 (2H, m), 7.97 (2H, d, J = 8.0 Hz), 7.60 (2H, m), 7.57 (2H, d, J = 8.0 Hz), 6.00 (1H, s).

1.3 X-ray crystallography

The X-ray diffraction data were collected on an Agilent Xcalibur Atlas Gemini ultra diffractometer with graphite-monochromated Mo Kα radiation (λ = 0.71073 Å) at room temperature. Absorption corrections were applied using a multi-scan method. The structure was solved by direct methods, and refined by full-matrix least-squares techniques on F^2 with the SHELXL-2016 program package.[1] The SQUEEZE instruction for removing the solvent molecules and counteranions in **Cd-L-COO** was employed to get the better refinement and data convergence. The solvent mask calculation using the SQUEEZE instruction indicated the presence of 220 electrons in a volume of 600 Å^3 in 1 void per unit cell. All the non-hydrogen atoms were refined with anisotropic displacement parameters. The hydrogen atoms attached to C atoms were placed by geometrical calculations, and their positions and thermal parameters were fixed during structural refinement. The topological structure of **Cd-L-COO** was obtained by using TOPOS 4.0 program. The empirical formula for **Cd-L-COO** was derived from the crystallographic data (Table S2) combining the results of EA and TGA.

1.4 Procedure for photocatalytic experiments

1.4.1 Photocatalytic experiments in air

The typical photocatalytic experiments were conducted on a multichannel photochemical reaction system. A mixture of photocatalyst, substrate, and acetonitrile in the special reaction vessel was irradiated by 365 nm light (light intensity: 298 mW cm^{-2}) under an air atmosphere. The catalytic system was kept at 26 °C by using the water circulating pump. The yield of product was analyzed by gas chromatograph (GC).

1.4.2 Photocatalytic experiments in N_2

The photocatalytic procedure operated in N_2 is similar to that in air, except that the catalytic reactions were carried out under a nitrogen atmosphere.

1.4.3 Photocatalytic experiments in O_2

The photocatalytic procedure operated in O_2 is similar to that in air, except that the catalytic reactions were carried out under an oxygen atmosphere.

1.4.4 Reversibility and stability of catalyst in the aerobic oxidation of alcohols

Following the aerobic oxidation of 4-methoxybenzyl alcohol (4-MBA) into 4-methoxybenzaldehyde (PAA) conducted under 365 nm light irradiation for 45 min in acetonitrile-water solution (4:1, v/v), the reaction mixture was subjected to centrifugation. The remaining solid was washed at least five times by acetonitrile to remove the substrate and product as much as possible, then used as the catalyst to study its reversibility in the selective oxidation of 4-MBA. The stability of catalyst was confirmed by comparing its PXRD patterns measured before and after the catalytic reaction.

1.4.5 Procedure for scavenger-quenching experiments

Besides photocatalyst, substrate, and acetonitrile, the corresponding scavenger was added into the special reaction vessel. Then the scavenger-quenching experiment was carried out under the same conditions as the photocatalytic experiment in air.

1.4.6 Calculation of turnover frequency (TOF)

TOF is obtained as the following equation:

TOF (h^{-1}) = (Con. × n_p)/(n_c × h)

Where n_p is the mole numbers of substrate, n_c is the mole numbers of active sites of catalyst, h is the reaction time.

1.5 Calculation of photochemical reaction kinetics

Photochemical reaction kinetics for **Cd-L-COO** in solid state are expressed as the following equation:

$$kt = \ln\left(\frac{A_0 - A_\infty}{A_t - A_\infty}\right)$$

Where *k* is the rate constant given by the equation, *t* is the irradiation time, A_0, A_∞ and A_t standing for the UV–Vis absorption values (715 nm) at the beginning, end, and a time *t* of the photochromic reaction, respectively.

Section 2. Additional schemes, figures, and tables

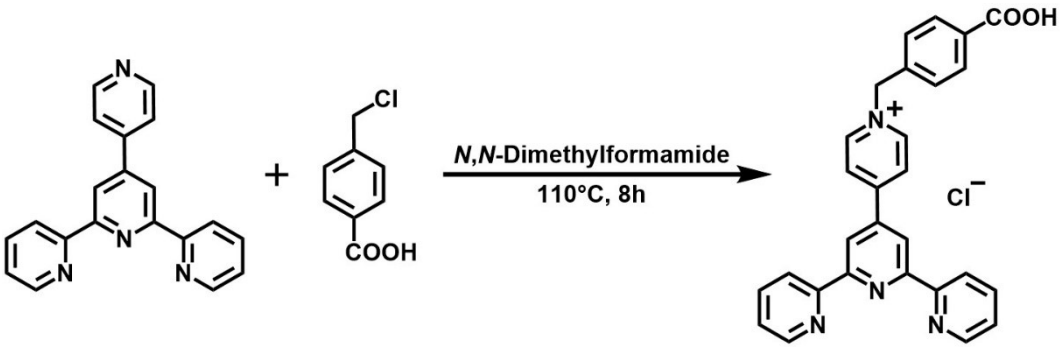

Scheme S1. Schematic diagram for synthesizing **L-COOH·Cl**.

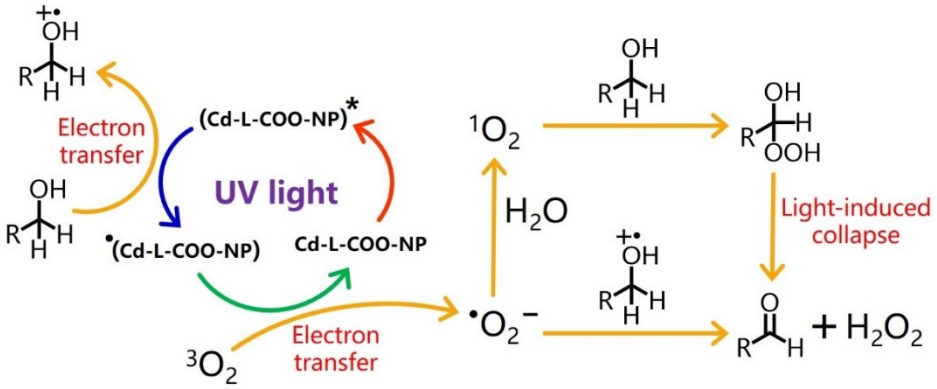

Scheme S2. Proposed reaction mechanism of **Cd-L-COO-NP** for the catalytic oxidation of alcohols in acetonitrile-water solution under an air atmosphere and 365 nm light.

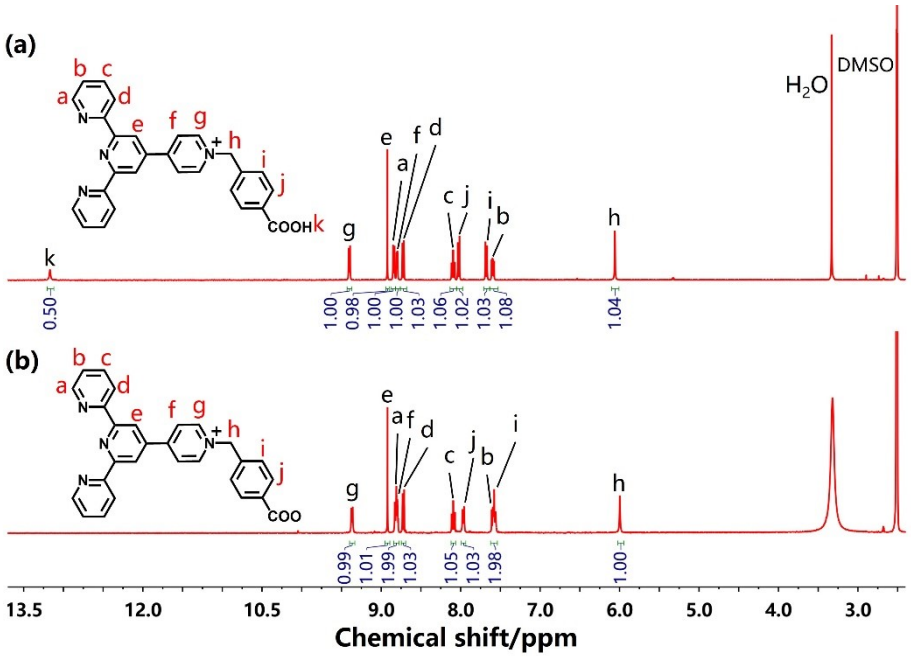

Fig. S1 (a) ^{1}H NMR spectra of **L-COOH·Cl** in DMSO-d_6 solution; (b) ^{1}H NMR spectra of **L-COO** in DMSO-d_6 solution.

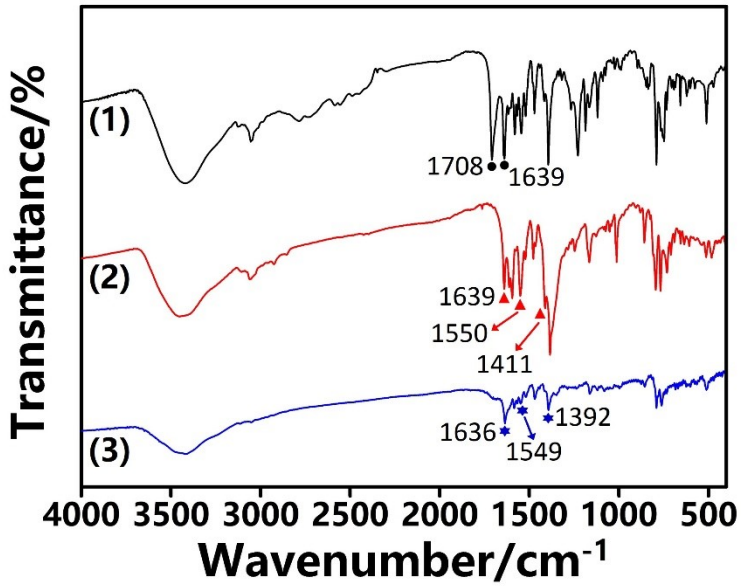

Fig. S2 IR spectra of (1) **L-COOH·Cl**. The peaks at 1708 and 1639 cm^{-1} are attributed to the C=O stretching vibration of the carboxyl group and the C=N stretching vibration of the pyridinium unit, respectively. (2) **Cd-L-COO**. A broadened characteristic band at 1385 cm^{-1} is attributed to the overlapping symmetric stretching vibrations of carboxylate groups and nitrate anions, thereby providing an evidence for the presence of nitrate ions in **Cd-L-COO**. (3) **L-COO**. By comparison with **L-COOH·Cl**, the disappearance of a strong peak at 1708 cm^{-1} indicates that the carboxyl groups in **L-COO** are fully deprotonated, where the asymmetric and symmetric stretching vibrations appear at 1549 and 1392 cm^{-1}, respectively.

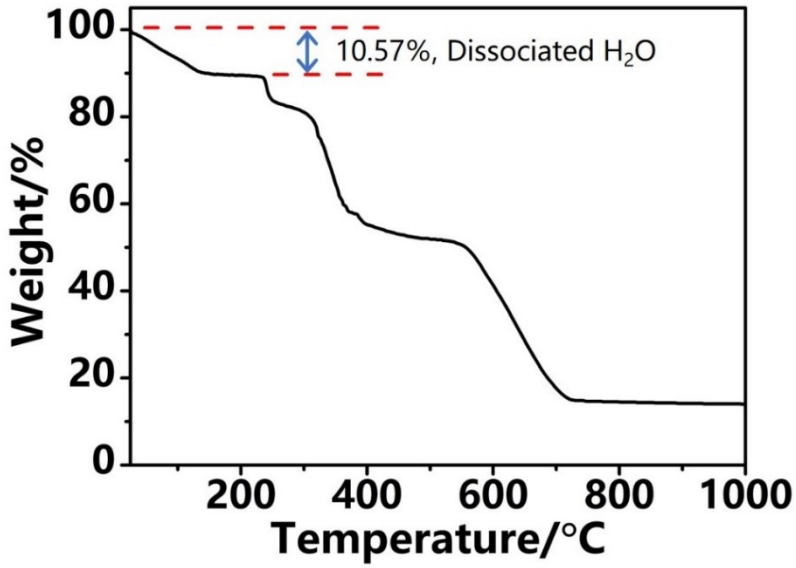

Fig. S3 Thermogravimetric analysis of **Cd-L-COO**. Four dissociated water molecules (10.57%) are released before 157 °C.

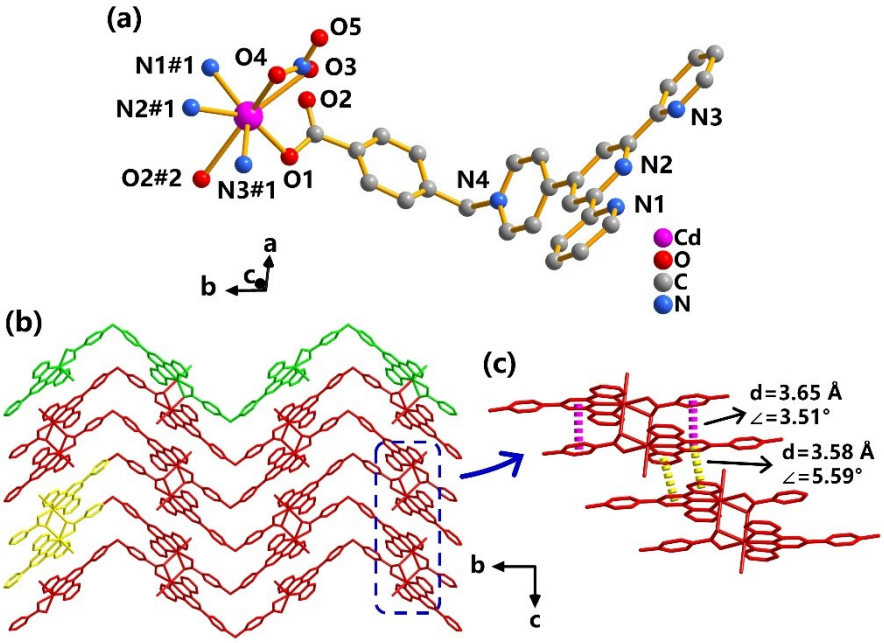

Fig. S4 (a) Coordination environment of Cd^{2+} centers in [Cd(L-COO)NO_3] component (hydrogen atoms and water molecules omitted for clarity). Symmetry codes: #1 1−x, 0.5+y, 1.5−z; #2 1−x, 2−y, 1−z. Each Cd^{2+} center adopts a seven-coordinate environment, bonded to three N and two O atoms from different **L-COO** ligands, as well as two O atoms from a nitrate anion. (b) The 2D layer in **Cd-L-COO**; (c) The corresponding distance and angle between the central pyridine and benzene rings involving the *inter*molecular CT interaction in the 2D layer.

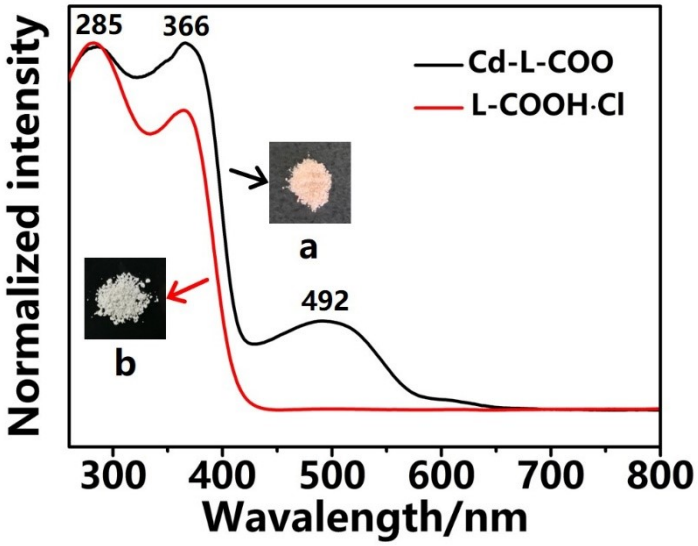

Fig. S5 UV-Vis diffuse reflectance absorption spectra of **Cd-L-COO** and **L-COOH·Cl**. The insert displays photographs of **Cd-L-COO** (a) and **L-COOH·Cl** (b). The absorption peak at 285 nm is attributed to the π-π* transition. The peak centered at 366 nm corresponds to the intramolecular charge transfer (CT) transition of **L-COO** ligand in **Cd-L-COO**, which is also observed in **L-COOH·Cl**. It must be noted that an additional peak (492 nm) in **Cd-L-COO** is a result of the *inter*molecular CT interaction generated by the crystal engineering.

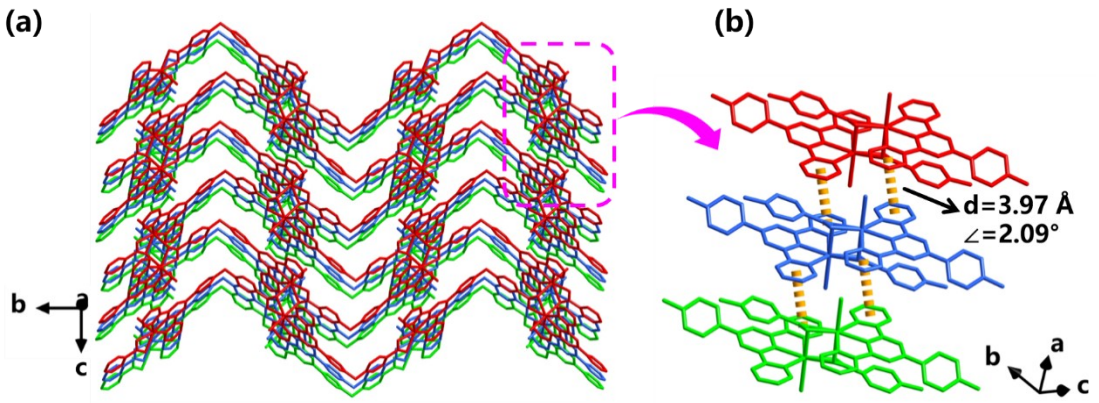

Fig. S6 (a) The 3D supramolecular framework formed *via* π-π stacking interaction; (b) The corresponding distance and angle between the peripheral pyridine rings involving π-π stacking interaction in the 3D supramolecular framework.

Fig. S7 Photographs showing photochromism of **Cd-L-COO** under 365 nm irradiation and its fading in the dark.

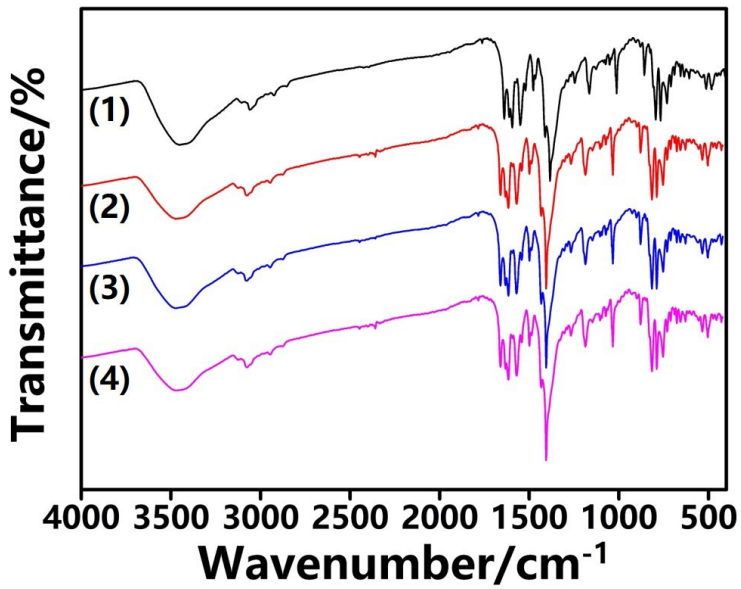

Fig. S8 IR spectra of (1) **Cd-L-COO** in as-synthesized. (2) **Cd-L-COO** after coloration. The almost unchanged peaks indicate that no photolysis occurs during the photochromic process. (3) **Cd-L-COO-NP30**. The almost unchanged peaks between **Cd-L-COO** and **Cd-L-COO-NP30** indicate that no structural transformation happens during the ultrasonic process. (4) **Cd-L-COO-NP30** after catalytic reaction. The almost unchanged peaks indicate that no structural transformation takes place after catalytic reaction.

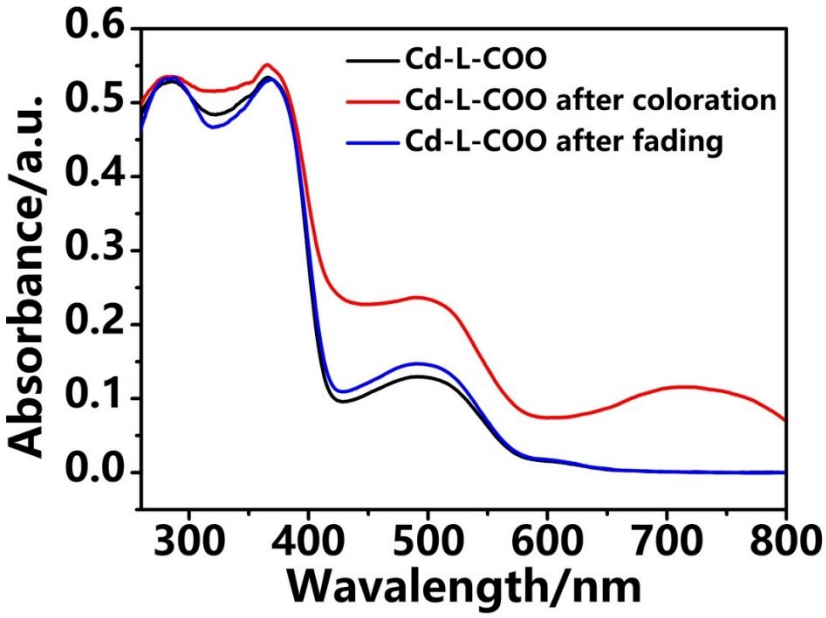

Fig. S9 UV-Vis diffuse reflectance absorption spectra of **Cd-L-COO** in air before (black line) or after (red line) 20 s of 365 nm light irradiation, and after fading completely in darkness (blue line).

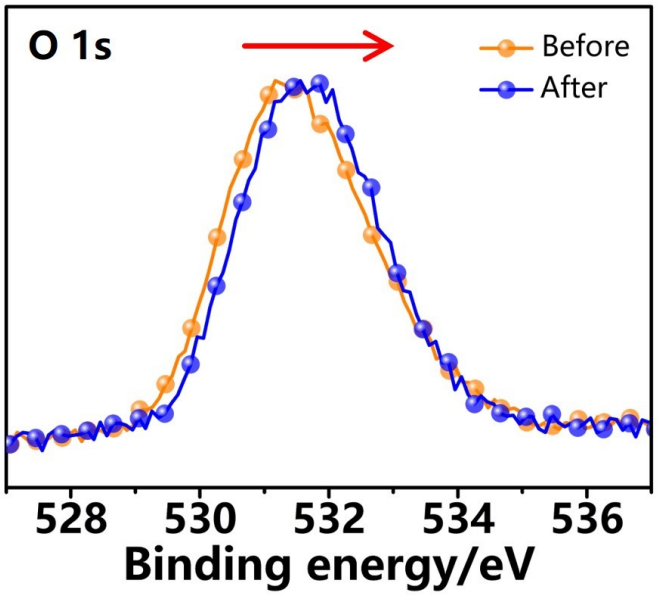

Fig. S10 Changes in XPS core-level spectra of **Cd-L-COO** for O 1s before and after 365 nm light irradiation.

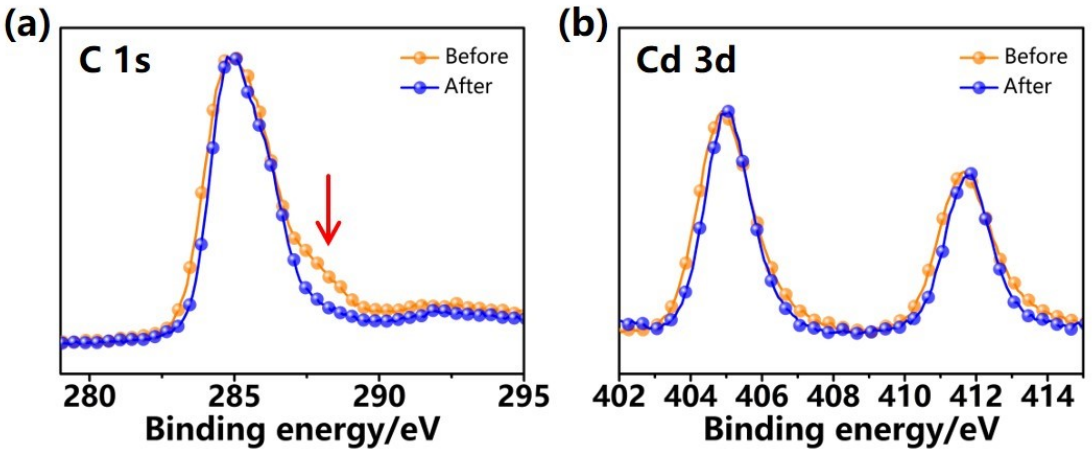

Fig. S11 Changes in XPS core-level spectra of **Cd-L-COO** for C 1s (a) and Cd 3d (b) before and after 365 nm light irradiation. The electron transfer from the carboxylate O atoms to the pyridinium N atoms has an effect on the C atoms of the pyridinium ring and carboxylate group, resulting in the variation of C 1s spectra. Since the carboxylate O atoms that coordinate with Cd^{2+} ion loss electrons, the Cd 3d core-level spectra are also affected and shift to the higher binding energy range.

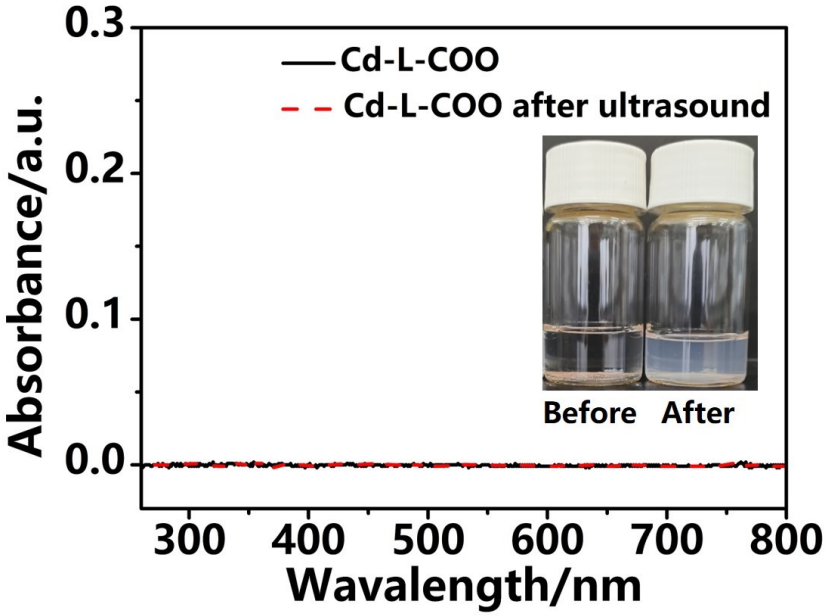

Fig. S12 UV-Vis absorption spectra of the supernatant obtained by centrifuging the mixture containing the same concentration of **Cd-L-COO** (0.01 g per 100 g of acetonitrile) before (black line) or after (red line) the ultrasonic treatment in acetonitrile. The insert illustrates the pictures about the mixture containing the same amount of **Cd-L-COO** before or after the ultrasonic treatment in acetonitrile. No absorbance is found during the range of 260-800 nm for the supernatant, proving that **Cd-L-COO** is scarcely soluble in acetonitrile.

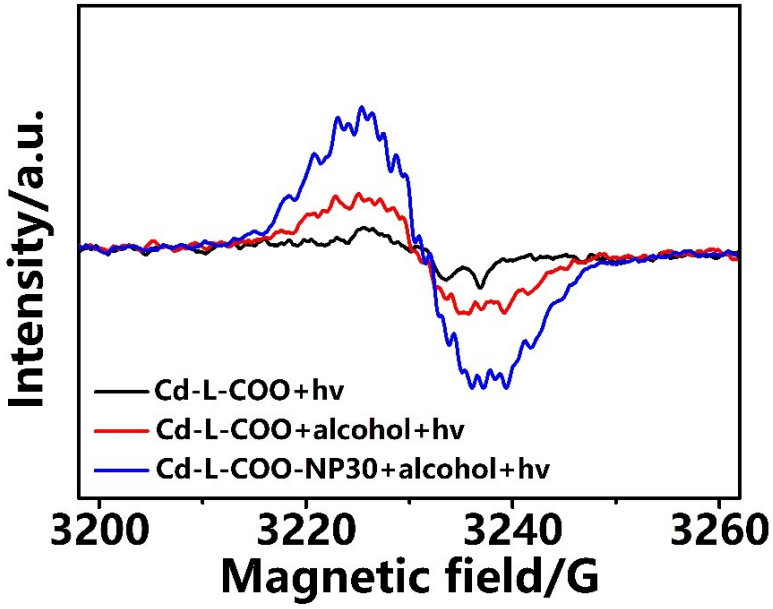

Fig. S13 ESR spectra of the same amount of **Cd-L-COO** (black line), **Cd-L-COO** after adding 4-MBA (red line), and **Cd-L-COO-NP30** after adding 4-MBA (blue line) under the same time of 365 nm light irradiation in 5 mL of acetonitrile under a nitrogen atmosphere.

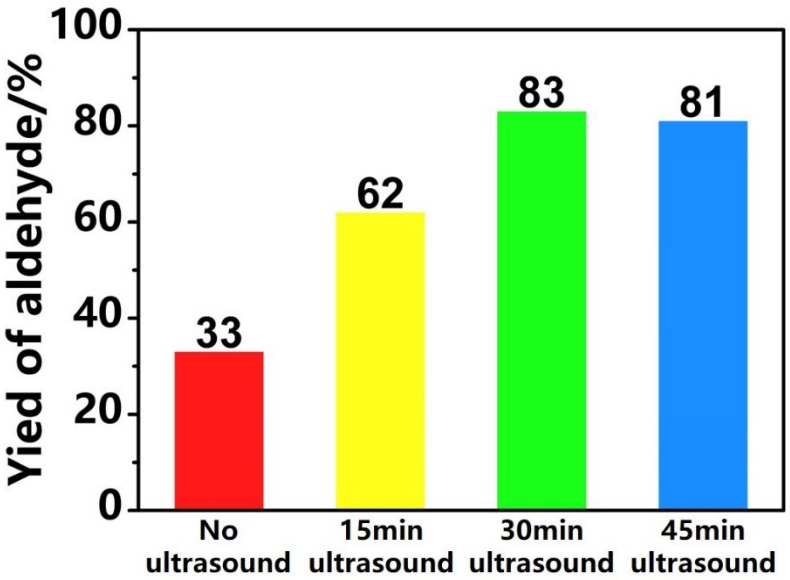

Fig. S14 Effect of ultrasonic time for **Cd-L-COO** on the yield of PAA during the oxidation of 4-MBA within 60 min in 5 mL of acetonitrile under 365 nm light.

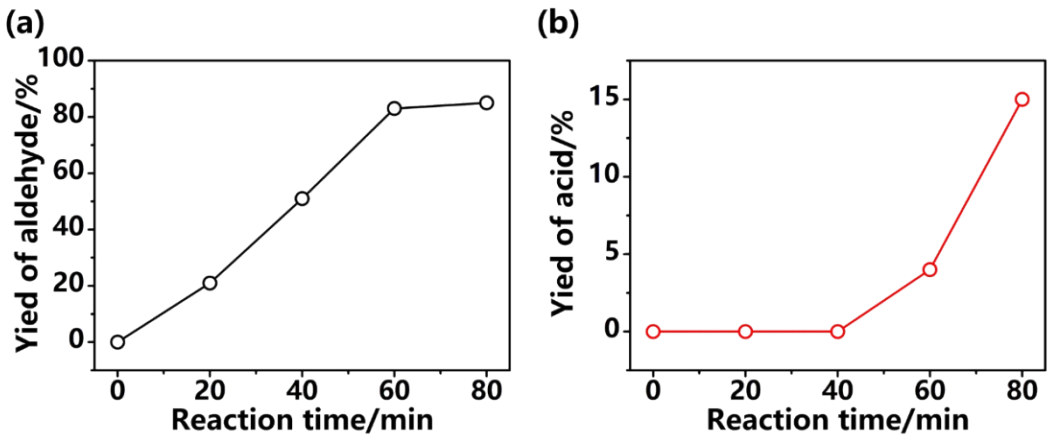

Fig. S15 (a) Yield of PAA obtained by using **Cd-L-COO-NP30** during the oxidation of 4-MBA within 80 min in 5 mL of acetonitrile under 365 nm light; (b) Yield of 4-methoxybenzoic acid obtained by using **Cd-L-COO-NP30** during the oxidation of 4-MBA within 80 min in 5 mL of acetonitrile under 365 nm light.

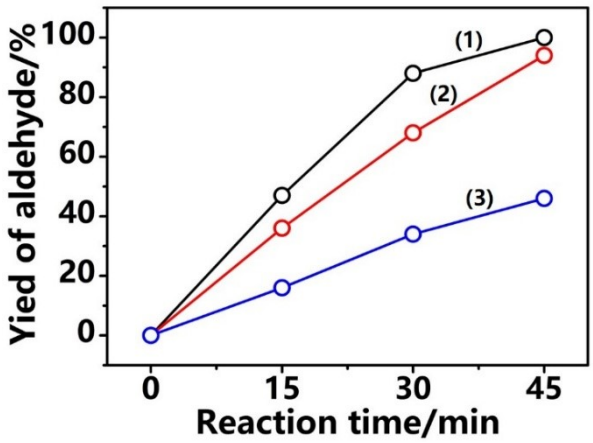

Fig. S16 Yield of PAA obtained by using **Cd-L-COO-NP30** during the oxidation of 4-MBA within 45 min in 5 mL of acetonitrile-water solution (4:1, v/v) (1), 5 mL of acetonitrile-water solution (3:2, v/v) (2), and 5 mL of water (3) under 365 nm light.

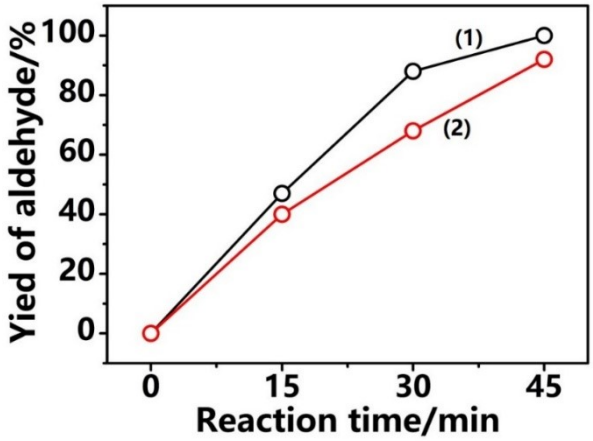

Fig. S17 Yield of PAA obtained by using **Cd-L-COO-NP30** (1) or **L-COO** (2) with the same number of active sites during the oxidation of 4-MBA within 45 min in 5 mL of acetonitrile-water solution (4:1, v/v) under 365 nm light.

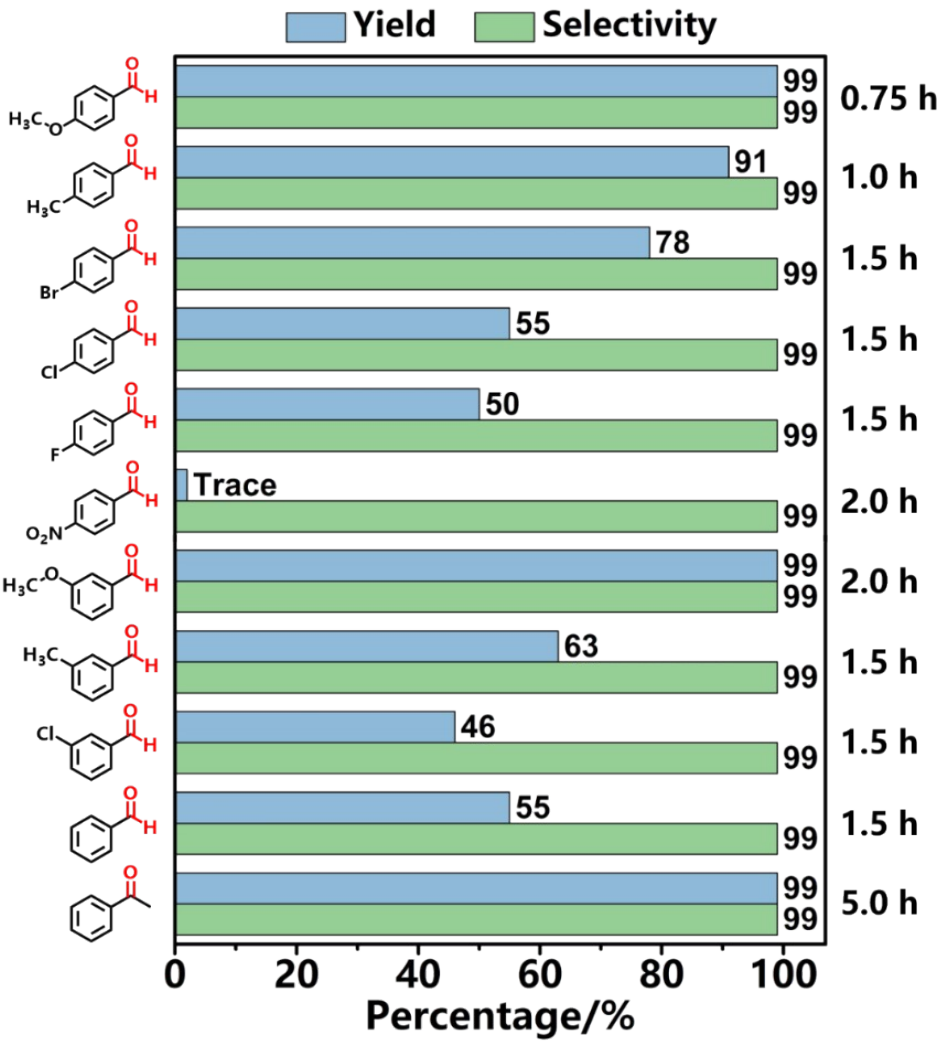

Fig. S18 Yield and selectivity of carbonyl compounds obtained by using **Cd-L-COO-NP30** in 5 mL of acetonitrile-water solution (4:1, v/v) during the oxidation of various aromatic alcohols under 365 nm light. The conversion of primary alcohols to the corresponding aldehydes becomes harder gradually as the electron-donating ability of *para* substituents decreases ($–OCH_3$ > $–CH_3$ > –Br > –Cl > –F > $–NO_2$) (Table S4, entries 1-10). Besides that, the *meta*-substituted aromatic alcohols are more difficult to be oxidized than those with the same substituents at the *para* position. About a half of benzyl alcohol is converted selectively into benzaldehyde within 1.5 h. Nevertheless, **Cd-L-COO-NP30** doesn't work in the catalytic oxidation of heteroaromatic, alicyclic or aliphatic alcohols (Table S4, entries 11-13). As for the secondary aromatic alcohol (1-phenylethanol), the yield is relatively low for the product of acetophenone in the first 2 h of light irradiation but reaches almost 100% after 5 h (Table S4, entries 14 and 15).

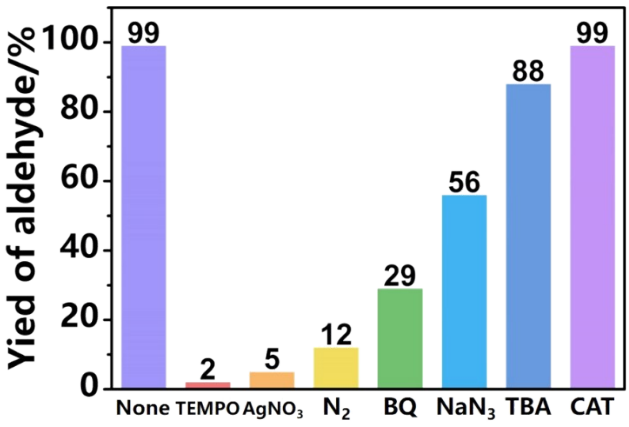

Fig. S19 Yield of PAA obtained by using **Cd-L-COO-NP30** in 5 mL of acetonitrile-water solution (4:1, v/v) under 365 nm light after adding various scavengers. The reactive species in the photooxidation of 4-MBA were probed using various scavengers. The sharp decline in PAA yield upon addition of TEMPO or $AgNO_3$ indicates that the reaction proceeds via a radical pathway involving electron transfer. The negligible conversion under N_2 highlights the essential role of O_2, further supported by ESR results showing that pyridinium radicals formed under N_2 vanish upon air exposure. These findings suggest that O_2 enables the pyridinium redox cycle and the generation of ROS. The inhibition effects of BQ and NaN_3, along with the ESR signals of DMPO-$^{\bullet}O_2^-$ and TEMP-$^1O_2$ adducts (Figs. S21 and S22), confirm $^{\bullet}O_2^-$ and $^1O_2$ as the principal ROS. A trace amount of $^{\bullet}OH$ detected in the acetonitrile-water system contributes slightly to alcohol oxidation, whereas H_2O_2, though present as a by-product (Fig. S23), is catalytically inactive.

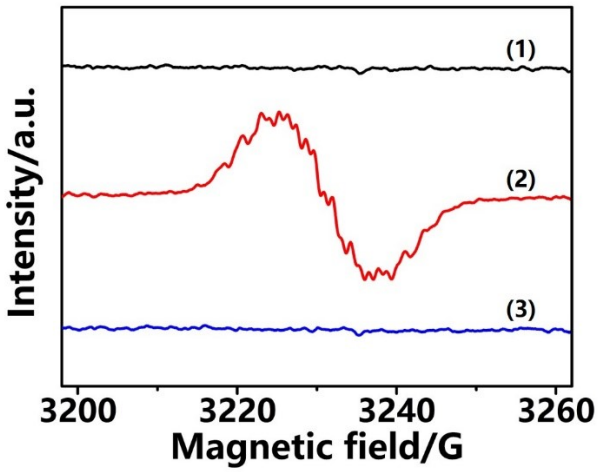

Fig. S20 ESR spectra of **Cd-L-COO-NP30** with 4-MBA in acetonitrile-water solution (4:1, v/v) under a nitrogen atmosphere without light irradiation (1), under a nitrogen atmosphere after 365 nm light irradiation (2), and under an air atmosphere after removing 365 nm light (3).

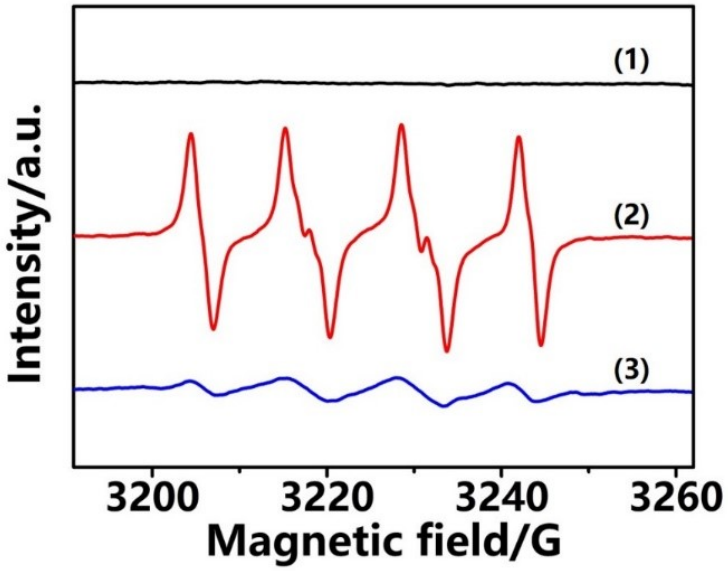

Fig. S21 ESR spectra of DMPO-$^{\bullet}O_2^-$ detected for **Cd-L-COO-NP30** and 4-MBA in the presence of DMPO in acetonitrile-water solution (4:1, v/v) under an air atmosphere without light irradiation (1), upon 365 nm light irradiation before (2) and after (3) adding BQ.

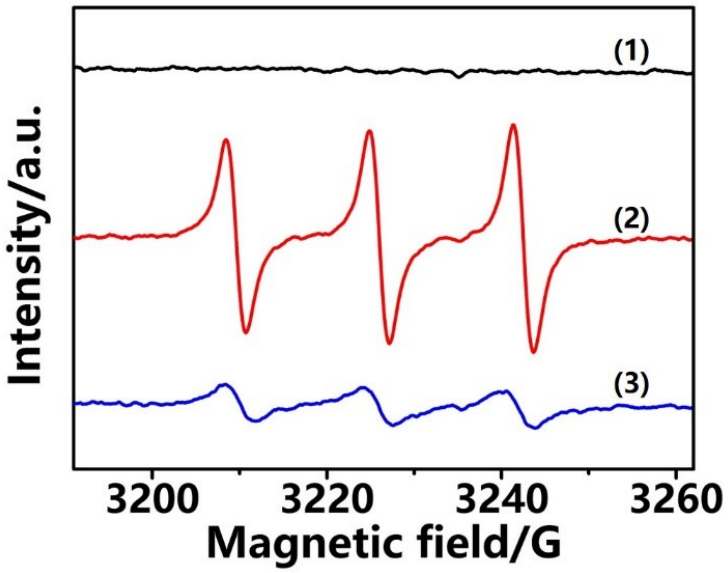

Fig. S22 ESR spectra of TEMP-$^1O_2$ detected for **Cd-L-COO-NP30** and 4-MBA in the presence of DMPO in acetonitrile-water solution (4:1, v/v) under an air atmosphere without light irradiation (1), upon 365 nm light irradiation before (2) and after (3) adding NaN_3.

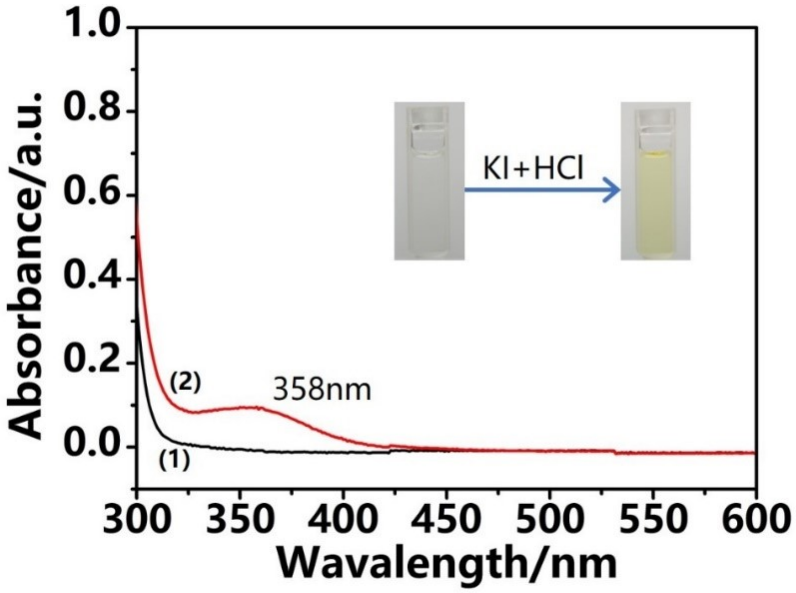

Fig. S23 UV-Vis absorption spectra of the photocatalytic reaction mixture before (1) and after (2) adding KI/HCl aqueous solution. The insert displays the color change of photocatalytic reaction mixture after adding KI/HCl aqueous solution. By contrast, an additional peak observed at 358 nm, which is attributed to the triiodide anion (I_3^-),[2] demonstrates the presence of H_2O_2.

Table S1. Crystallographic data and refinement parameters for **Cd-L-COO**.

Compound name	**Cd-L-COO**
CCDC	2520285
Empirical formula	$C_{28}H_{29}CdCl_{0.64}N_{4.36}O_{8.07}$
Formula weight	690.89
Crystal system	Monoclinic
Space group	$P12_1/c1$
T (K)	293(2)
a (Å)	9.217(14)
b (Å)	29.385(3)
c (Å)	11.251(12)
α (°)	90
β (°)	106.903(13)
γ (°)	90
V (Å^3)	2915.6(7)
Z	4
D_{calcd} (g cm^{-3})	1.617
Absorption coefficient (mm^{-1})	0.871
F(000)	1446.051
Reflections collected	15914
Reflections unique	5119
R_{int}	0.0385
GOF on F^2	1.0240
R_1, wR_2 ($I > 2\sigma(I)$)	0.0615, 0.1706
R_1, wR_2 (all data)	0.0929, 0.1907
Largest diff. peak and hole (e Å^{-3})	0.6061, –0.5716

Table S2. Exploration for the aerobic oxidation of 4-MBA by using **Cd-L-COO**.[a]

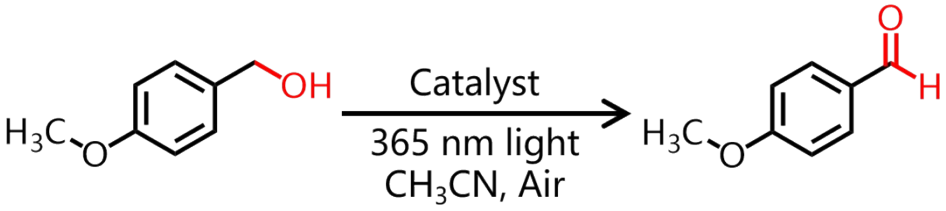

Entry	Catalyst dosage (mg)	Selectivity (%)[b]	Yield (%)[b]	TOF (h^{-1})
1	1.0	>99	8	1.4
2	2.0	>99	12	2.0
3	3.0	>99	21	3.6
4	4.0	>99	33	5.6
5[c]	–	>99	Trace	–
6[d]	4.0	>99	Trace	–

[a]Reaction conditions: the mixture containing 4-MBA (0.1 mmol) and **Cd-L-COO** in 5 mL of acetonitrile is irradiated by 365 nm light (light intensity: 298 mW cm^{-2}) for 60 min under an air atmosphere. [c]No catalyst. [d]No light source.

Table S3. Exploration for the aerobic oxidation of 4-MBA by using **Cd-L-COO-NP30**.[a]

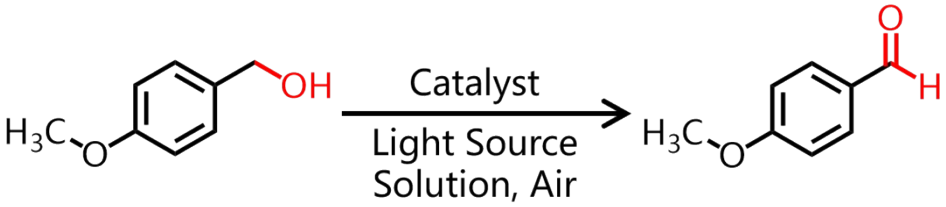

Entry	Reaction solution	Light source[b]	Selectivity (%)[c]	Yield (%)[c]	TOF (h^{-1})
1	Acetonitrile-water (4:1, v/v)	365 nm	>99	>99	22.7
2	Acetonitrile-water (3:2, v/v)	365 nm	>99	94	21.4
3	Water	365 nm	>99	46	10.4
4	Acetonitrile-water (4:1, v/v)	395 nm	>99	54	12.3
5	Acetonitrile-water (4:1, v/v)	White light	>99	Trace	–
6[d]	Acetonitrile-water (4:1, v/v)	365 nm	>99	92	20.9

[a]Reaction conditions: the mixture containing 4-MBA (0.1 mmol) and **Cd-L-COO-NP30** (4.0 mg) in 5 mL of solution is irradiated by different light sources for 45 min under an air atmosphere. [b]The light intensity of 365 nm light, 395 nm light, and white light is 298 mW cm^{-2}, 607 mW cm^{-2}, and 307 mW cm^{-2}, respectively. [c]Selectivity and yield were calculated by the GC data. [d]By using **L-COO** (3.0 mg) as the catalyst.

Table S4. Selective oxidation of various alcohols to the corresponding carbonyl compounds by **Cd-L-COO-NP30** under the optimum conditions.[a]

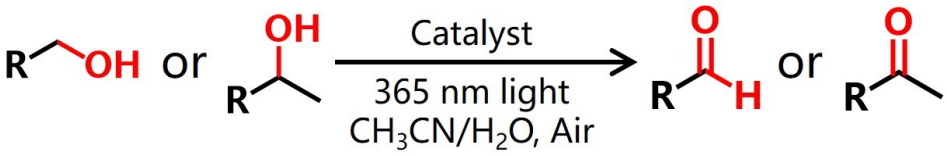

Entry	Substrate	Product	Time (h)	Sel./Yld. (%)[b]	TOF (h^{-1})
1	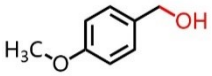	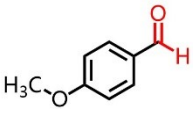	0.75	>99/>99	22.7
2	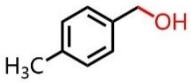	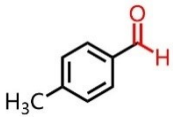	1.0	>99/91	15.5
3	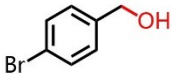	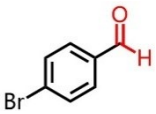	1.5	>99/78	8.9
4	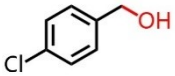	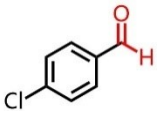	1.5	>99/55	6.2
5	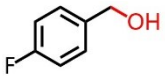	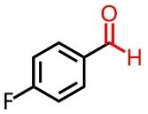	1.5	>99/50	5.7
6	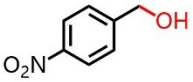	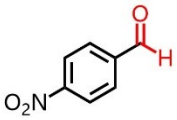	2.0	>99/Trace	–
7	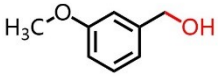	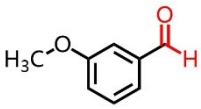	2.0	>99/>99	8.5
8	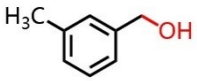	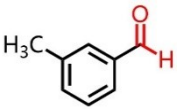	1.5	>99/63	7.2
9	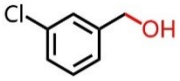	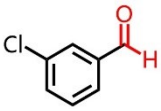	1.5	>99/46	5.2
10	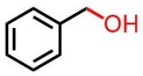	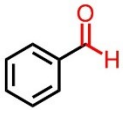	1.5	>99/55	6.2
11	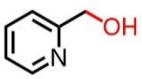	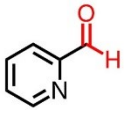	2.5	>99/9	0.6
12	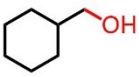	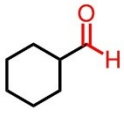	2.5	>99/5	0.3

13		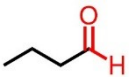	2.5	>99/6	0.4
14	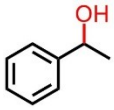	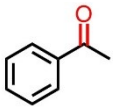	2.0	>99/49	4.2
15	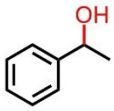	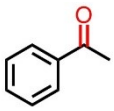	5.0	>99/>99	3.4

[a]Reaction conditions: the mixture containing alcohol (0.1 mmol) and **Cd-L-COO-NP30** (4.0 mg) in 5 mL of acetonitrile-water solution (4:1, v/v) is irradiated by 365 nm light (light intensity: 298 mW cm^{-2}) under an air atmosphere. [b]Sel. (selectivity) and Yld. (yield) were calculated by the gas chromatography (GC) data.

Table S5. Comparison between **Cd-L-COO-NP30** and other heterogeneous catalysts reported recently for the transformation of 1-phenylethanol into acetophenone.

Size	Material	Entry	Catalyst	Metal	Additive	Oxidant	Conditions	Time (h)	Yld. (Con./Sel.)[a] (%)
Micron or larger level	CPs	1[3]	TJU-68-NHPI	Zr	TBN	O_2	80 °C	5	>99 (–/–)
		2[4]	HENU-1	Cu, W	–	TBHP	60 °C	3	97 (–/–)
		3[5]	MIL-125(Ti)-NH_2	Ti, Cu	–	TBHP	80 °C	5	>99 (>99/>99)
		4[6]	NENU-9	V, Mo, Cu	–	TBHP	100 °C	7	– (97/–)
		5[7]	NH_2-MIL-125(Ti)	Ti	–	O_2	420-780 nm light	40	46 (46/>99)
	COFs	6[8]	CTF-Th	–	BTF	O_2	460 nm light, RT[b]	4	90 (90/>99)
	Carbon nitride	7[9]	g-C_3N_4	–	–	O_2	Visible light	3	57 (57/>99)
		8[10]	CD-C_3N_4	–	–	O_2	>400 nm light, 30 °C	24	40.2 mM[c]
	Metal oxide	9[11]	SMO	Sr, Mn	–	O_2	80 °C	1.5	>99 (–/–)
	Metal sulfide	10[12]	Ni/CdS	Ni, Cd	–	–	Ar gas, blue LED light	20	94 (97/97)
	Composi-te	11[13]	NH_2-MIL-125@TAPB-PDA-3	Ti	–	O_2	>420 nm light	30	71 (71/>99)
		12[14]	ARS-TiO_2	Ti	–	Air	Green LED light, RT[b]	2	84 (87/96)
		13[15]	TiO_2-(PW_{12}-TH)$_8$	Ti, W	BTF	O_2	Visible light, RT[b]	2.5	27 (27/>99)
		14[16]	20 wt% MnO_X/SiO_2	Mn, Si	–	O_2	100 °C	6	22 (–/–)
		15[17]	STA/Ag_2S/CdS	Ag, Cd, Si, W	–	O_2	>420 nm light	0.5	– (>99/–)
Nano level	CPs	16[18]	Cu-MOF-2	Cu	TEMPO, Na_2CO_3	O_2	120 °C	16	Trace (–/–)
		17[19]	MIL-101(Cr)-guanidine-Fe	Cr, Fe	–	H_2O_2	RT[b]	8	98 (–/–)
	Metal oxide	18[20]	Rh-STO-600	Rh, Sr, Ti, Pt	–	–	Ar gas, >400 nm light, 14 °C	6	35 (35/>99)

	19[21]	2.5BWO	W	–	O_2	>420 nm light, 25 °C	6	– (>80/–)
Metal sulfide	20[22]	CdS-CD	Cd	–	–	Ar gas, 450 nm light, 25 °C	180	– (–/93)
Metal nanopart-icle	21[23]	Au/MD-COL	Au	–	TBHP	Microwave, 150 °C	2	>99 (–/–)
Composi-te	22[24]	Fe_3O_4 /$Cu_3(btc)_2$	Fe, Cu	TEMPO, Na_2CO_3	O_2	75 °C	12	7 (7/>99)
	23[25]	1.0 mol% Au@UiO-66(NH_2)	Au, Zr	–	O_2	100 °C	1	74 (–/–)
	24[26]	0.5 wt% Au-Pd(2:8) /$ZnIn_2S_4$	Au, Pd, Zn, In	–	O_2	Visible light, RT[b]	10	52 (59/88)
	25[27]	Au-TiO_2	Au, Ti	–	TBHP	400-700 nm light, RT[b]	6	96 (–/–)
	26[28]	Au /$Zn_{0.7}Cu_{0.3}O$	Au, Zn, Cu	–	O_2	120 °C	5	>99 (>99/>99)
	27[29]	MSNPs-NH2@H[1]	Si, Co	K_2CO_3	$Na_2S_2O_8$	300 nm light, RT[b], sonication	8	>99 (–/–)
Our work	28	**Cd-L-COO-NP30**	Cd	–	Air	365 nm light, RT[b]	5	>99 (>99/>99)

[a]Yld., Con., and Sel. represent yield, conversion, and selectivity. [b]RT represents room temperature. [c]There is only the concentration of product in the literature.

Table S6. Research of reactive species in the oxidation of 4-MBA by adding various scavengers.[a]

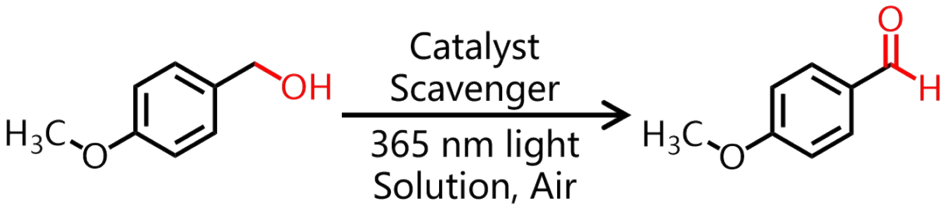

Entry	Scavenger	Notes	Yield (%)[b]
1	–	–	>99
2[c]	TEMPO	Radical scavenger	2
3[d]	$AgNO_3$	Electron scavenger	5
4[e]	–	–	12
5[f]	BQ	Superoxide radical scavenger	29
6[g]	NaN_3	Singlet oxygen scavenger	56
7[h]	TBA	Hydroxyl radical scavenger	88
8[i]	CAT	Hydrogen peroxide scavenger	>99

[a]Reaction conditions: the mixture containing 4-MBA (0.1 mmol), **Cd-L-COO-NP30** (4.0 mg), and scavenger in 5 mL of acetonitrile-water solution (4:1, v/v) is irradiated by 365 nm light (light intensity: 298 mW cm^{-2}) for 45 min under an air atmosphere. [b]Yield was calculated by the GC data. [c]TEMPO (0.04 mol L^{-1}): 2,2,6,6-tetramethylpiperidine-*N*-oxyl. [d]$AgNO_3$ (0.01 mol L^{-1}): silver nitrate. [e]Under a nitrogen atmosphere. [f]BQ (0.01 mol L^{-1}): benzoquinone. [g]NaN_3 (0.01 mol L^{-1}): sodium azide. [h]TBA (0.01 mol L^{-1}): tert-butyl alcohol. [i]CAT (200 U mL^{-1}): catalase.

Notes and references

1 G. M. Sheldrick, *Acta Cryst.*, 2008, **A64**, 112-122.

2 S. Merouani, O. Hamdaoui, F. Saoudi and M. Chiha, *J. Hazard. Mater.*, 2010, **178**, 1007-1014.

3 M. Wang, G. Liang, Y. Wang, T. Fan, B. Yuan, M. Liu, Y. Yin and L. Li, *Chem. Eur. J.*, 2021, **27**, 9674-9685.

4 D. Li, Q. Xu, Y. Li, Y. Qiu, P. Ma, J. Niu and J. Wang, *Inorg. Chem.*, 2019, **58**, 4945-4953.

5 S. Daliran, A. Santiago-Portillo, S. Navalón, A. R. Oveisi, M. Álvaro, R. Ghorbani-Vaghei, D. Azarifar and H. García, *J. Colloid Interface Sci.*, 2018, **532**, 700-710.

6 X. H. Li, Y. W. Liu, S. M. Liu, S. Wang, L. Xu, Z. Zhang, F. Luo, Y. Lu and S. X. Liu, *J. Mater. Chem. A*, 2018, **6**, 4678-4685.

7 Z. Wu, X. Huang, H. Zheng, P. Wang, G. Hai, W. Dong and G. Wang, *Appl. Catal., B*, 2018, **224**, 479-487.

8 W. Huang, B. C. Ma, H. Lu, R. Li, L. Wang, K. Landfester and K. A. I. Zhang, *ACS Catal.*, 2017, **7**, 5438-5442.

9 X. Wang, S. Blechert and M. Antonietti, *ACS Catal.*, 2012, **2**, 1596-1606.

10 W. Zhang, A. Bariotaki, I. Smonou and F. Hollmann, *Green Chem.*, 2017, **19**, 2096-2100.

11 S. Kawasaki, K. Kamata and M. Hara, *ChemCatChem*, 2016, **8**, 3247-3253.

12 Z. Chai, T. T. Zeng, Q. Li, L. Q. Lu, W. J. Xiao and D. Xu, *J. Am. Chem. Soc.*, 2016, **138**, 10128-10131.

13 G. Lu, X. Huang, Y. Li, G. Zhao, G. Pang and G. Wang, *J. Energy. Chem.*, 2020, **43**, 8-15.

14 X. Li, J. L. Shi, H. Hao and X. Lang, *Appl. Catal., B*, 2018, **232**, 260-267.

15 X. Yang, H. Zhao, J. Feng, Y. Chen, S. Gao and R. Cao, *J. Catal.*, 2017, **351**, 59-66.

16 K. Nakamura, N. Ichikuni, T. Hara, T. Kojima and S. Shimazu, *Catal. Today*, 2020, **352**, 250-254.

17 I. Kornarakis, I. N. Lykakis, N. Vordos and G. S. Armatas, *Nanoscale*, 2014, **6**, 8694-8703.

18 Y. Qi, Y. Luan, J. Yu, X. Peng and G. Wang, *Chem. Eur. J.*, 2015, **21**, 1589-1597.

19 A. Shaabani, R. Mohammadian, H. Farhid, M. Karimi Alavijeh and M. M. Amini, *Catal. Lett.*, 2019, **149**, 1237-1249.

20 G. Zhao, G. W. Busser, C. Froese, B. Hu, S. A. Bonke, A. Schnegg, Y. Ai, D. Wei, X. Wang, B. Peng and M. Muhler, *J. Phys. Chem. Lett.*, 2019, **10**, 2075-2080.

21 J. Wang, H. Liang, C. Zhang, B. Jin and Y. Men, *Appl. Catal., B*, 2019, **256**, 117874.

22 J. Wang, Y. X. Feng, M. Zhang, C. Zhang, M. Li, S. J. Li, W. Zhang and T. B. Lu, *CCS Chem.*, 2020, **2**, 81-88.

23 S. A. C. Carabineiro, A. P. C. Ribeiro, J. G. Buijnsters, M. Avalos-Borja, A. J. L. Pombeiro, J. L. Figueiredo and L. M. D. R. S. Martins, *Catal. Today*, 2020, **357**, 22-31.

24 J. Li, H. Gao, L. Tan, Y. Luan and M. Yang, *Eur. J. Inorg. Chem.*, 2016, **2016**, 4906-4912.

25 Y. Luan, Y. Qi, H. Gao, N. Zheng and G. Wang, *J. Mater. Chem. A*, 2014, **2**, 20588-20596.
26 C. Feng, X. Yang, Z. Sun, J. Xue, L. Sun, J. Wang, Z. He and J. Yu, *Appl. Surf. Sci.*, 2020, **501**, 144018.
27 N. Gogoi, G. Borah, P. K. Gogoi and T. R. Chetia, *Chem. Phys. Lett.*, 2018, **692**, 224-231.
28 W. Wang, Y. Xie, S. Zhang, X. Liu, L. Zhang, B. Zhang, M. Haruta and J. Huang, *Chin. J. Catal.*, 2019, **40**, 1924-1933.
29 I. Guerrero, A. Saha, J. A. M. Xavier, C. Vinas, I. Romero and F. Teixidor, *ACS Appl. Mater. Interfaces*, 2020, **12**, 56372-56384.